AD-A117 159 ARMY MISSILE COMMAND REDSTONE ARSENAL AL F/G 20/5
MICOM PROGRAM IN LIGHT CONTROL BY LIGHT.(U)
JUN 82 C M BOWDEN

UNCLASSIFIED NL

END
DATE FILMED
8 82
DTIC

MICOM PROGRAM IN LIGHT CONTROL BY LIGHT (U)

CHARLES M. BOWDEN, DR.
RESEARCH DIRECTORATE, US ARMY MISSILE LABORATORY
US ARMY MISSILE COMMAND
REDSTONE ARSENAL, ALABAMA 35898

1. INTRODUCTION

Superfluorescence (1) is the phenomenon whereby a collection of atoms or molecules is prepared initially in a state of complete inversion, and then allowed to undergo relaxation by collective, spontaneous decay. This produces pulses of anomalous intensity (proportional to the square of the density of active atoms) and of anomalous, temporal duration (inversely proportional to the density). Since Dicke's initial work (2), there has been a preponderance of theoretical and experimental work dealing with this process (3).

With the exception of the more recent work of Bowden and Sung (4), all theoretical treatments have dealt exclusively with the relaxation process from a prepared state of complete inversion in a two-level manifold of atomic energy levels, and thus do not consider the dynamical effects of the pumping process. Yet, all reported experimental work (3,5-10) has utilized optical pumping on a minimum manifold of three atomic or molecular energy levels by laser pulse injection into the nonlinear medium, which subsequently fluorescesces.

It was pointed out by Bowden and Sung (4) that for a system otherwise satisfying the conditions for superfluorescent emission, unless the characteristic superradiance time (1), τ_R, is much greater than the pump pulse temporal duration, τ_p, i.e., $\tau_R >> \tau_p$, the process of coherent optical pumping on a three-level system can have dramatic effects on the SF. This is a condition which has not been realized over the full range of reported data.

In this paper, we present calculational results and analysis for the effects of coherent pump dynamics, propagation, transverse and diffraction effects on SF emission from an optically-pumped three-level system. The full, nonlinear, co-propagational aspects of the injected pump pulse, together with the SF which evolves are explicitly treated in the calculation.

Not only do our results relate strongly to previous calculations and experimental results in SF, but we introduce and demonstrate a new concept in nonlinear light-matter interactions, which we call light control by light. We show how characteristics of the SF can be controlled by specifying certain characteristics of the injection pulse. This leads to possible applications in laser pulse control and shaping, nonlinear optical information encoding, and unique pulsed LADAR and millimeter wavelength sources.

In the next section, the model upon which the calculation is based is presented and the algorithm used in the simulation is outlined. Results of the calculation are presented and discussed in Section 3. The last section is used to summarize the results and cite implications and to discuss future work.

2. MODEL FOR THREE-LEVEL SUPERFLUORESCENCE

The model upon which the calculation is based is comprised of a collection of identical three-level atoms, each having the energy level scheme shown in Figure 1. The $1 \leftrightarrow 3$ transition is induced by a coherent electromagnetic field injection pulse of frequency ω_0 nearly tuned to the indicated transition. The properties of this pumping pulse are specified initially in terms of the initial and boundary conditions. The transition $3 \leftrightarrow 2$ evolves by spontaneous emission at frequency ω. It is assumed that the energy level spacing is such that $\epsilon_3 > \epsilon_2 >> \epsilon_1$ so that the fields of frequencies ω_0 and ω can be treated by separate wave equations. The energy levels $2 \leftrightarrow 1$ are not coupled radiatively due to parity considerations.

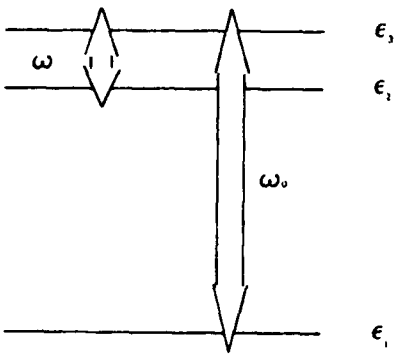

Figure 1. Model three-level atomic system and electric field tunings under consideration. For the results reported here, the injected pulse is tuned to the $1 \leftrightarrow 3$ transition.

Further, we neglect spontaneous relaxation in the $3 \leftrightarrow 1$ transition, and spontaneous relaxation in the $3 \leftrightarrow 2$ transition is simulated by the choice of a small, but nonzero, initial transverse polarization characterized by the parameter $\dagger_0 \sim 10^{-3}$. Our results do not depend upon nominal variations of this parameter. The initial condition is chosen consistent with the particular choice of $\dagger_0$, with nearly all the population in the ground state, and the initial values of the other atomic variables chosen consistently (4,11).

We use the electric dipole and rotating wave approximation and couple the atomic dipole moments to classical field amplitudes which are determined from Maxwell's equations. The Hamiltonian which describes the field-matter interaction for this system comprising N atoms (4), is

$$H = \hbar \sum_{r=1}^{3} \sum_{j=1}^{N} \varepsilon_{rj} R_{rr}^{(j)} - \frac{i\hbar}{2} \sum_{j=1}^{N} \left[\Omega^{(j)} R_{32}^{(j)} \, e^{-i(\omega t - \underline{k}\cdot\underline{r}_j)} - \Omega^{(j)*} R_{23}^{(j)} e^{i(\omega t - \underline{k}\cdot\underline{r}_j)} \right]$$

$$- \frac{i\hbar}{2} \sum_{j=1}^{N} \left[\omega_R^{(j)} R_{31}^{(j)} \quad e^{-i(\omega_o t - \underline{k}_o\cdot\underline{r}_j)} - \omega_R^{(j)*} R_{13}^{(j)} \, e^{i(\omega t - \underline{k}_o\cdot\underline{r}_j)} \right] \quad (1)$$

The first term on the right-hand side of Eq. (1) is the free atomic system Hamiltonian, with atomic level spacings ε_{rj}, r = 1,2,3; j=1,2,...,N. The second term on the right-hand side describes the interaction of the atomic system with the fluorescence field associated with the $3 \leftrightarrow 2$ transition, whereas the last term on the right in Eq.(1) describes the interaction between the atomic system and the coherent pumping field. The fluorescence field and the pumping field have amplitudes $\Omega^{(j)}$ and $\omega_R^{(j)}$, respectively, in terms of Rabi frequency, at the position of the j^{th} atom, $\underline{r}_j$. The respective wave vectors of the two fields are k and k_o and the carrier frequencies are ω and ω_o. It is assumed that the electromagnetic field amplitudes vary insignificantly over the atomic dimensions and that all of the atoms remain fixed during the time frame of the dynamical evolution of the system.

The atomic variables in Eq. (1) are the canonical operators (4) $R_{k\ell}^{(j)}$ which obey the Lie algebra defined by the commutation rules (12-14)

$$\left[R_{ij}^{(m)} \, , \, R_{\ell k}^{(n)} \right] = R_{ik}^{(m)} \, \delta_{\ell j} \, \delta_{mn} - R_{\ell j}^{(m)} \, \delta_{ik} \, \delta_{mn} \quad (2)$$

i,j = 1,2,3; m,n = 1,2,...,N. The Rabi rates, $\Omega^{(j)}$ and $\omega_R^{(j)}$ are given in terms of the electric field amplitudes $E^{(j)}$ and $E_o^{(j)}$, respectively, and the matrix elements of the transition dipole moments, $u_{32}^{(j)}$ and $u_{31}^{(j)}$ by

$$\Omega^{(j)} = \frac{E^{(j)}u_{32}^{(j)}}{\hbar} \quad ; \quad \omega_R^{(j)} = \frac{E_o^{(j)}u_{31}^{(j)}}{\hbar} \quad , \tag{3a,b}$$

where we have considered only one linear polarization for the two fields and propagation in the positive z direction.

It is convenient to introduce a new set of variables in terms of the old ones. We let

$$W_{k\ell} = R_{kk} - R_{\ell\ell} \ , \ k > \ell \quad ; \quad R_{k\ell} = \frac{1}{2}\left(U_{k\ell} + i\, V_{k\ell}\right) \ , \ k > \ell, \tag{4a,b}$$

where $U_{k\ell}, V_{k\ell}$, and $W_{k\ell}$ are real variables, and $U_{k\ell} = U_{\ell k}$, $V_{k\ell} = V_{\ell k}$,

$$\Omega = X + iY \quad ; \quad \omega_R = X_o + iY_o \quad , \tag{4c,d}$$

where X, Y, X_o and Y_o are real variables which are functions of both space and time.

The equations of motion for the atomic variables are calculated according to the commutation relation

$$i\hbar\, \dot{R}_{k\ell}^{(j)} = \left[H, R_{k\ell}^{(j)}\right] \quad . \tag{5}$$

If the transformation, Eqs. (4) is applied to the hierarchy of Eqs. (5), the resulting equations of motion for the real variables $\left\{W_{k\ell}, U_{k\ell}, V_{k\ell}\right\}$ are

$$\dot{W}_{31} = \frac{1}{2}\left\{XU_{32} - YV_{32}\right\} + \left\{X_oU_{31} - Y_oV_{31}\right\} - \gamma_{11}\left[W_{31} - W_{31}^{(e)}\right] , \tag{6a}$$

$$\dot{W}_{32} = \left\{XU_{32} - YV_{32}\right\} + \frac{1}{2}\left\{X_oU_{31} - Y_oV_{31}\right\} - \gamma_{11}\left[W_{32} - W_{32}^{(e)}\right] , \tag{6b}$$

$$\dot{U}_{32} = -\delta V_{32} - XW_{32} + \frac{1}{2}\left[X_oU_{12} - Y_oV_{12}\right] - \gamma_1 U_{32} , \tag{6c}$$

$$\dot{V}_{32} = \delta U_{32} + YW_{32} - \frac{1}{2}\left[X_oV_{21} + Y_oU_{21}\right] - \gamma_1 V_{32} , \tag{6d}$$

$$\dot{U}_{31} = \Delta V_{31} + \frac{1}{2}\left[XU_{21} + YV_{21}\right] - X_oW_{31} - \gamma_1 U_{31} , \tag{6e}$$

$$\dot{V}_{31} = -\Delta U_{31} + \frac{1}{2}\left[XV_{21} - YU_{21}\right] + Y_oW_{31} - \gamma_1 V_{31} , \tag{6f}$$

$$\dot{U}_{21} = \Delta V_{21} - \frac{1}{2}\left[XU_{31} - YV_{31}\right] - \frac{1}{2}\left[X_o U_{32} - Y_o V_{32}\right] - \gamma_\perp U_{21} \ , \qquad (6g)$$

$$\dot{V}_{21} = -\Delta U_{21} - \frac{1}{2}\left[XV_{31} + YU_{31}\right] - \frac{1}{2}\left[X_o V_{32} + Y_o U_{32}\right] - \gamma_\perp V_{21} \ , \qquad (6h)$$

where

$$\Delta^{(j)} = \varepsilon_{33}^{(j)} - \omega_o \ , \quad \Delta^{(j)} = \varepsilon_{22}^{(j)} + \omega - \omega_o \ , \ \varepsilon_{11} = 0. \qquad (7)$$

In obtaining Eqs. (6), we have made use of the invariant, tr S = I,

$$I \equiv R_{11}^{(j)} + R_{22}^{(j)} + R_{33}^{(j)} \ . \qquad (8)$$

It is noted that $\dot{I} = 0$ is satisfied identically in Eqs. (6) for $\gamma_{11} \to 0$. For $\gamma_{11} \neq 0$, the condition, Eq. (8) together with Eqs. (6) constitutes the statement of conservation of atomic density, i.e., particle number.

The Eqs. (6) are coupled to Maxwell's equations through the polarizations associated with each transition field. It is easily determined that the Maxwell's equations in dimensionless form in the rotating wave and slowly-varying envelope approximations can be written in the following form

$$\mathcal{F}_p^{-1}\nabla_\rho^2 \begin{Bmatrix} -\tilde{X}_o \\ \tilde{Y}_o \end{Bmatrix} + \frac{\partial}{\partial \eta_p} \begin{Bmatrix} \tilde{Y}_o \\ \tilde{X}_o \end{Bmatrix} = d \begin{Bmatrix} -U_{31} \\ V_{31} \end{Bmatrix} \ , \qquad (9a)$$

$$\mathcal{F}_s^{-1}\nabla_\rho^2 \begin{Bmatrix} -\tilde{X} \\ \tilde{Y} \end{Bmatrix} + \frac{\partial}{\partial \eta_s} \begin{Bmatrix} \tilde{Y} \\ \tilde{X} \end{Bmatrix} = d \begin{Bmatrix} -U_{32} \\ V_{32} \end{Bmatrix} \ , \qquad (9b)$$

where the variables $\tilde{X}$, $\tilde{Y}$, $\tilde{X}_o$, $\tilde{Y}_o$ are the same as those defined in Eqs. (4), but in units of $\gamma_\perp$. In the above equations, we have assumed cylindrical symmetry, thus

$$\nabla_\rho^2 = \frac{1}{\rho}\frac{\partial}{\partial \rho}\left(\rho \frac{\partial}{\partial \rho}\right) \ .$$

The first term on the left-hand side in Eqs. (9a,b) accounts for transverse effects with normalized radial coordinate $\rho = r/r_p$ where r is the radial distance and r_p is a characteristic spatial width. In Eqs. (9), $\eta_{p_s} = z\, g_{eff_{p_s}}$ where $g_{eff_{p_s}}$ is the on-axis effective gain,

$$g_{eff_{p_s}} = \frac{\left\{\frac{\omega_o}{\omega}\right\}\left\{\frac{\mu_{31}}{\mu_{32}}\right\}^2 N}{n\hbar c} T_2 \qquad (10)$$

where N is the atomic number density (assumed longitudinally homogeneous) and η is the index of refraction assumed identical for each transition wavelength. The quantity

$$d = N(r)/N_o \qquad (11)$$

governs the relative radial population density distribution for active atoms. Equations (9) are written in the retarded time, τ, frame where $\tau = t - n\,z/c$. From this point on, $\cdot$ in Eqs. (6) is taken to be $\cdot = \partial/\partial\tau$. Finally, the first factors on the first terms in Eqs. (9) are the reciprocals of the "gain length" Fresnel numbers defined by

$$\mathcal{F}_{p_s} \equiv \frac{2\pi r_p^2}{\lambda_{p_s} g_{eff_{p_s}}^{-1}} \quad . \qquad (12)$$

It is seen from Eqs. (9) that for sufficiently large Fresnel number, $\mathcal{F}$, the corrections due to transverse effects become negligible. The "gain length" Fresnel numbers $\mathcal{F}$ are related to the usual Fresnel numbers $F = 2\pi r_p^2/\lambda L$, where L is the length of the medium, by

$$\mathcal{F}/F = g_{eff}L \quad , \qquad (13)$$

i.e., the total gains of the medium. In the computations, diffraction is explicitly taken into account by the boundary condition that $\rho = \rho_{max}$ corresponds to completely absorbing walls.

The initial conditions are chosen to establish a small, but nonzero transverse polarization for the $3 \leftrightarrow 2$ transition with almost the entire population in the ground state. This requires the specification of two small dimensionless parameters, $\varepsilon \sim 10^{-3}$, for the ground state initial population deficit, and $\delta \sim 10^{-3}$ for the tipping angle for the initial transverse polarization for the $3 \leftrightarrow 2$ transition. The derivation for the initial values for the various matrix elements is presented elsewhere (15).

3. CALCULATIONAL RESULTS AND ANALYSIS

Calculational methods developed earlier (16) and discussed elsewhere (17,18) were applied to the model presented in the last section to compute

the effects on SF pulse evolution for various initial conditions for the injected (pump) pulse. The results presented here demonstrate many facets of the control and shaping of the SF signal by control of the input signal initial characteristics.

In Figure 2 is shown results of the numerical calculation for the transverse integrated intensity profiles for the co-propagating SF and injected pulses at a penetration depth of $z = 5.3$ cm in the nonlinear medium. These profiles correspond to what would be observed with a wide aperture, fast, energy detector. The pumping pulses are labeled by capital letters and the corresponding SF pulses are labeled by the corresponding lower case letters. Each set of curves represents a different initial on-axis area for the pump pulse, i.e., curve A) is the reshaped pump pulse at $z = 5.3$ cm which had its initial on-axis area specified as $\theta_p = \pi$, and curve a) is the resulting SF pulse which has evolved. All other parameters are identical for each set of pulses. The initial conditions for the atomic medium is that nearly all the population is in the ground state ε_1 at $\tau = 0$, and a small, but nonzero macroscopic polarization exists between levels ε_3 and ε_2. These two conditions are specified by two parameters ε and δ, respectively, and we have chosen $\delta = \varepsilon = 10^{-3}$ self-consistently in terms of the initial values of the matrix elements for the entire system. These initial conditions are uniform for the atomic medium and are the same for all results reported here. Notice that we have neglected spontaneous relaxation in the pump transition, $1 \leftrightarrow 3$, relative to the SF transition, $3 \leftrightarrow 2$. This is justified due to our choice of relative oscillator strengths (see Figure 2 caption).

These results clearly indicate the coherence effect of the initial pump pulse area on the SF signal which evolves. Notice that the peak intensity of the SF pulses increases monatomically with initial on-axis area for the pump pulse. This is caused by self-focusing due to transverse coupling and propagation. For instance, a 2π-injection pulse would generate a very small SF response compared to an initial π-injection pulse for these conditions at relatively small penetration z, or for the corresponding case in one spacial dimension. The delay time τ_p between the pump pulse peak and the corresponding SF pulse peak is very nearly inversely proportional to the input pulse area. The temporal SF pulse full width at half maximum (FWHM), τ_w is approximately invariant with respect to the injection pulse area.

Figure 3 shows the effect upon the SF pulse of variation in the initial temporal width at half maximum intensity for the pumping pulse. As the initial temporal width of the injected pulse τ_w becomes smaller, the SF delay time τ_D increases whereas the peak SF intensity decreases and the SF temporal width τ_s remains very closely fixed. It is clear from these results that there exists a linear relationship between the time delay τ_D,

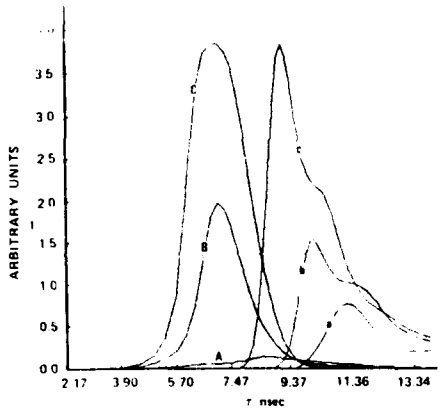

Figure 2. Radially integrated normalized intensity profiles for the SF and injected pulse at z = 5.3 cm penetration depth for 3 different values for the initial on-axis injection pulse area θ_p. The SF pulses are indicated by a, b, and c, whereas the corresponding injected pump pulses are labeled by A, B, and C. The injected pulses are initially Gaussian in r and τ with widths (FWHM) r_o = 0.24 cm and τ_p = 4 nsec, respectively. The level spacings are such that $(\varepsilon_3-\varepsilon_1)/(\varepsilon_3-\varepsilon_2)$ = 126.6. The effective gain for the pump transition g_p = 17 cm^{-1} and that for the SF transition, g_s = 291.7 cm^{-1}. The gain length Fresnel numbers for the two transitions are $\mathcal{F}_p$ = 16800 and $\mathcal{F}_s$ = 2278. The relaxation and dephasing times are taken as identical for all transitions, and are given as T_1 = 80 nsec and T_2 = 70 nsec, respectively. The injected pulse initial on-axis areas are: A) $\theta_p = \pi$; B) $\theta_p = 2\pi$; C) $\theta_p = 3\pi$.

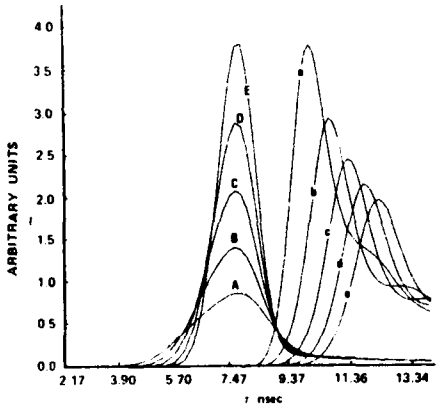

Figure 3. Radially integrated normalized intensity profiles for the SF and injected pulses at z = 5.3 cm penetration depth for 5 different values for the initial temporal width of the injected pulse. The initial on-axis area of the injected pulse is $\theta_p = \pi$ and the pump transition and SF effective gains are g_p = 17.5 cm^{-1} and g_s = 641.7 cm^{-1}, respectively. All other parameters except for the Fresnel numbers, are the same as those for Figure 2. The injected pulse initial temporal widths at half maximum are: A) τ_w = 4 nsec; B) τ_w = 3.3 nsec; C) τ_w = 2.9 nsec; D) τ_w = 2.5 nsec; E) τ_w = 2.2 nsec.

between the peak SF intensity and the corresponding pump pulse intensity, and the initial temporal width τ_w of the pump pulse. This is in qualitative agreement with the analytical prediction made in reference 4b, Eq. 5.1, based upon mean field theory. These results emphasize the importance of the initiating pulse characteristics in SF pulse evolution, and the effect of SF pulse narrowing with approximate pulse shape invariance by increasing the initial temporal width of the injected pulse. It is emphasized that all other parameters, including the initial value for the injected pulse on-axis area, are identical among these sets of curves.

The initial radial width, r_p, of the injected pulse was varied and the effect upon the SF pulse evolution is shown in Figure 4. There is clearly indicated an optimum value for r_p for which the SF peak intensity is a maximum and the SF temporal width τ_s is a minimum. If the relation, Eq. (13) is used in conjunction with the values of the parameters given in Figure 4 and its caption, it is seen that optimization occurs for a value for the conventional Fresnel number F_S for the SF transition, $F_S \simeq 1$. Thus, from Eq. (13) and $F_S = 1$, we have

$$\mathcal{F}_S = g_S z_{max} \tag{14}$$

for the gain-length Fresnel number. Since $F_S \sim 1/z$ the implication is that Eq. (14) gives the penetration depth, z_{max}, at which the SF peak intensity reaches a maximum in terms of the ratio $\mathcal{F}_S/g_S$. Since this takes both transverse and diffraction explicitly into account as well as propagation, this is indeed a profound statement.

Further insight into the implication of Eq. (14) can be obtained by considering a one-spacial dimension analogy. If the linear field loss is taken to be entirely due to diffraction, then the one-dimensional linear loss κ_S corresponding to the two-dimensional case specified by $\mathcal{F}_S$, is given by

$$\kappa_S = \frac{\lambda_S}{2\pi r_p^2} \quad . \tag{15}$$

Then, from Eq. (12)

$$\mathcal{F}_S = g_S/\kappa_S \tag{16}$$

is the effective gain, g_S, to loss, κ_S, ratio. From the condition, Eq. (14),

$$z_{max} = (\kappa_S^{-1}) \quad , \tag{17}$$

i.e., z_{max} is the penetration depth at which the SF peak intensity is a maximum, and corresponds to one effective diffraction length, as

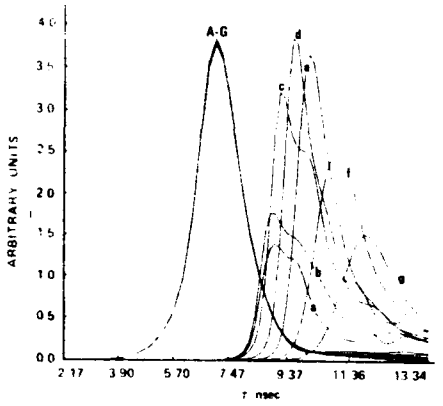

Figure 4. Radially integrated normalized intensity profiles for the SF and injected pulses at z = 5.3 cm penetration depth for 7 different values for the injected pulse initial radial width at half maximum r_p. The initial on-axis area θ_p of the injection pulse is $\theta_p = 2\pi$; the SF effective gain $g_s = 758.3\ cm^{-1}$ and the pump transition effective gain $g_p = 14.6\ cm^{-1}$; all other parameters are the same as for Figure 2. The initial radial widths at half maximum for the injected pulses are: a) $r_p = 0.57$ cm; b) $r_p = 0.43$ cm; c) $r_p = 0.24$ cm; d) $r_p = 0.18$ cm; e) $r_p = 0.15$ cm; f) $r_p = 0.11$ cm; g) $r_p = 0.09$ cm. The corresponding "gain length" Fresnel numbers are: a) $\mathcal{F}_p = 82876$, $\mathcal{F}_s = 34010$; b) $\mathcal{F}_p = 46898$, $\mathcal{F}_s = 19244$; c) $\mathcal{F}_p = 14428$, $\mathcal{F}_s = 5922$; d) $\mathcal{F}_p = 8326$, $\mathcal{F}_s = 3416$; e) $\mathcal{F}_p = 5602$, $\mathcal{F}_s = 2298$; f) $\mathcal{F}_p = 3422$, $\mathcal{F}_s = 1404$; g) $\mathcal{F}_p = 2082$, $\mathcal{F}_s = 854$.

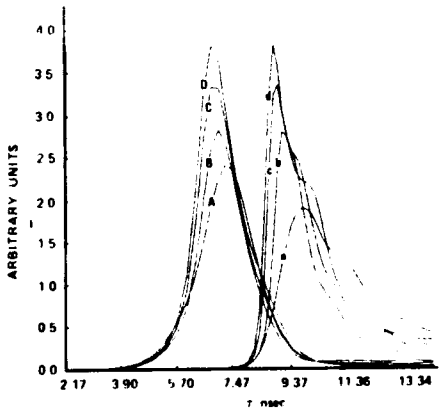

Figure 5. Radially integrated normalized intensity profiles for the SF and injected pulses at z = 5.3 cm penetration depth for 4 different values for the injected pulse initial radial shape parameter ν (see text). The initial on-axis area θ_p of the injected pulse is $\theta_p = 2\pi$ and the SF effective gain $g_s = 758.3\ cm^{-1}$, whereas the effective gain for the pump transition $g_p = 14.6\ cm^{-1}$. All other parameters are the same as for Figure 2. The initial radial shape parameters for the injected pulses are: A) $\nu = 1$; B) $\nu = 2$; C) $\nu = 3$; D) $\nu = 4$.

defined by Eq. (15). Carrying the one-dimensional analogy one step further, Eq. (16) used in Eq. (13) gives

$$F = (\kappa z)^{-1} \quad . \tag{18}$$

From Eqs. (16) and (18) we have exhibited the significance of the Fresnel numbers $\mathcal{F}$ and F in terms of diffraction loss, i.e., $\mathcal{F}$ can be thought of as gain to loss ratio, Eq. (16), whereas F can correspondingly be thought of as the reciprocal of the strength of the diffraction loss, Eq. (18).

The effect on SF pulse evolution of variation of the initial radial shape of the initiating pulse is shown in Figure 5. The shape parameter ν is defined in terms of the initial condition for the pump transition field amplitude, $\omega_R(r)$,

$$\omega_R(r) = \omega_R(o) \exp\left[-(r/r_p)^{\nu}\right] . \tag{19}$$

Thus, for $\nu = 2$, the initial amplitude of the injected pulse is radially Gaussian, whereas for $\nu = 4$, it is radially super-Gaussian. We see from the results presented in Figure 5 that as the initial radial shape of the injected pulse becomes broader, i.e., larger values for ν , the peak intensity of the SF pulse generated becomes larger, and the width τ_s diminishes. It is emphasized that all other parameters, including the initial values for the radial and temporal widths are invariant among these sets of curves.

The response of SF pulse evolution to changes in the initial temporal shape of the injection pulse is shown in Figure 6 which compares the effect of a Gaussian initial temporal shape for the pump pulse, identified by the temporal shape parameter, $\sigma = 2$, with that of a super-Gaussian identified by $\sigma = 4$. As for the radial distribution discussed previously, the temporal shape parameter σ is defined in terms of the initial condition for the pump transition field amplitude $\omega_R(\tau)$,

$$\omega_R(\tau) = \omega_R(o) \exp\left[-(\tau/\tau_p)^{\sigma}\right] . \tag{20}$$

Again, it is seen that the broader initial pump pulse causes an increase in the peak SF intensity and a reduction in the delay time τ_D and SF pulse width τ_s.

Finally, Figure 7 shows the effect of variation of the density ρ of active atoms. The effective gains, g_S and g_p, are changed proportionally, corresponding to a density variation ρ . The ratio of the SF intensities is $I_c/I_b = 1.76$ and $I_b/I_a = 2.06$; these ratios are larger than the

//

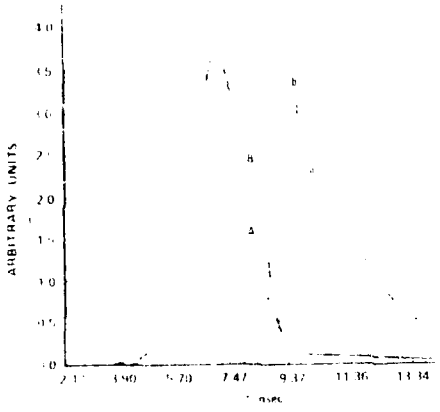

Figure 6. Radially integrated normalized intensity profiles for the SF and injected pulses at z = 5.3 cm penetration depth for two different values for the injected pulse initial temporal shape parameter σ (see text). The initial on-axis area θ_p of the injected pulse is $\theta_p = 2\pi$, and the SF effective gain $g_S = 641.7$ cm^{-1}. All other parameters are the same as for Figure 4(c). The initial radial shape parameters for the injected pulses are: a) $\sigma = 2$; b) $\sigma = 4$.

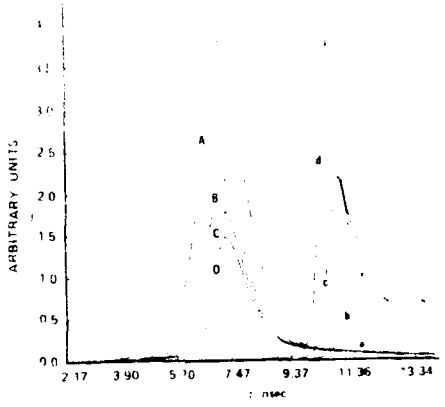

Figure 7. Radially integrated normalized intensity profiles for the SF and injected pulses at z = 5.3 cm penetration depth for three different values for the density ρ of atoms. The on-axis initial area θ_p for the injected pulse is $\theta_p = 2\pi$. Except for the effective gains and Fresnel numbers, the values for all other parameters are the same as for Figure 4(c). For each set of curves, the gain values are: a) $g_S = 525.0$ cm^{-1}; $g_p = 26.3$ cm^{-1}; b) $g_S = 641.7$ cm^{-1}, $g_p = 32.1$ cm^{-1}; c) $g_S = 758.3$ cm^{-1}, $g_p = 37.9$ cm^{-1}. The corresponding Fresnel numbers are: a) $\mathcal{F}_p = 25992$, $\mathcal{F}_s = 4100$; b) $\mathcal{F}_p = 31724$, $\mathcal{F}_s = 5010$; c) $\mathcal{F}_p = 37465$, $\mathcal{F}_s = 5922$.

corresponding density ratios squared (1), $(\rho_c/\rho_b)^2 = 1.40$ and $(\rho_b/\rho_a)^2 = 1.49$. This difference may be due to self-focusing, especially since the values of the effective gains used in this case are quite high. However, the ratio of the temporal widths, τ_W, (FWHM), is within 15% of the corresponding inverse ratios of the densities; the same is true for the delay time, τ_D, of the SF intensity peak with respect to the pump intensity peak. These results compare qualitatively reasonably well with the mean field predictions for SF in two-level systems initially prepared in a state of complete inversion (1).

4. CONCLUSIONS

The results presented here clearly demonstrate the coherence and deterministic effects on SF pulse evolution of injection pump pulse initial characteristics and conditions. It is suggested that effects of the type discussed here may have in fact been operative in SF experiments and their results which were published earlier (5-10).

Furthermore, and perhaps of greater importance, we have demonstrated the control and shaping of the SF pulse which evolves, by specification of particular initial characteristics and conditions for the pumping pulse which is injected into the nonlinear medium to initiate SF emission. These manifestations and others of the same class, we call the control of light by light via a nonlinear medium. This phenomenon constitutes a method for nonlinear information encoding, or information transfer, from the injection pulse characteristics to corresponding SF pulse characteristics which evolve due to propagation and interaction in the nonlinear medium.

Work is now in progress to incorporate the effects of quantum statistics of the SF spontaneous relaxation process (19). We are in the process of further determination and analysis of the nonlinear interaction between two co-propagating pulses resonantly, as well as nonresonantly, interacting by a nonlinear medium (19).

ACKNOWLEDGEMENT

Continued and valued collaboration with F. P. Mattar, Y. Claude and M. Cormier is gratefully acknowledged.

REFERENCES

1. R. Bonifacio and L. A. Lugiato, Phys. Rev. A11, 1507 (1975); A12, 587 (1975).

2. R. H. Dicke, Phys. Rev. 93, 99 (1954).

3. See papers and references in Cooperative Effects in Matter and Radiation, edited by C. M. Bowden, D. W. Howgate and H. R. Robl, Plenum, New York, (1977). "Swept-gain Superradiance in CO_2-pumped CH_3F", J. J. Ehrlich, C. M. Bowden, S. H. Lehmigk, A. T. Rosenberger and T. A. DeTemple, in Coherence and Quantum Optics IV, edited by L. Mandel and E. Wolf, Plenum, New York, p. 903 (1978). "MIRADCOM Program in Swept-gain Super-Radiance", D. W. Howgate, C. M. Bowden and J. J. Ehrlich, US Army Science Conference Proceedings, June (1978), First Prize.

4. C. M. Bowden and C. C. Sung, Phys. Rev. A18, 1558 (1978); Phys. Rev. A20, 2033 (1979).

5. N. Skribanowitz, J. P. Herman, J. C. MacGillivray and M. S. Feld, Phys. Rev. Lett. 30, 309 (1973).

6. H. M. Gibbs, Q. H. F. Vrehen and H. M. J. Hickspoors, Phys. Rev. Lett. 39, 547 (1977).

7. Q. H. F. Vrehen, in Cooperative Effects in Matter and Radiation, edited by C. M. Bowden, D. W. Howgate and H. R. Robl, Plenum, New York, p. 79 (1977).

8. M. Gross, C. Fabre, P. Pillet and S. Haroche, Phys. Rev. Lett. 36, 1035 (1976).

9. A. Flusberg, F. Mossberg and S. R. Hartmann, in Cooperative Effects in Matter and Radiation, edited by C. M. Bowden, D. W. Howgate and H. R. Robl, Plenum, New York, p. 37, (1977).

10. A. T. Rosenberger and T. A. DeTemple, Phys. Rev. A24, 868 (1981).

11. F. T. Hioe and J. H. Eberly, Phys. Rev. Lett. 47, 838 (1981).

12. R. Gilmore, Lie Groups, Lie Algebras, and Some of Their Applications, Wiley, New York, Chapter 6, Section 2, (1974).

13. R. Gilmore, C. M. Bowden and L. M. Narducci, Phys. Rev. A12, 1019 (1975).

14. R. Gilmore, C. M. Bowden and L. M. Narducci, "c-Number Representation for Multilevel Systems and the Quantum-Classical Correspondence", in Quantum Statistics and the Many-Body Problem, edited by S. B. Trickey, W. R. Kirk and J. W. Dufty, Plenum, New York, (1975).

15. F. P. Mattar and C. M. Bowden, "Coherent Pump Dynamics and Pulse Evolution in Three-level Superfluorescence and Control of Light by Light", in Multiphoton Processes, edited by C. D. Cantrell, Springer-Verlag, New York, to appear, (1982).

16. F. P. Mattar and M. C. Newstein, in Cooperative Effects in Matter and Radiation, edited by C. M. Bowden, D. W. Howgate and H. R. Robl, Plenum, New York, p. 139 (1977).

17. F. P. Mattar, in Optical Bistability, edited by C. M. Bowden, M. Ciftan and H. R. Robl, Plenum, New York, p. 503 (1981); in Proceedings, Tenth Simulation and Modeling Conference, Pittsburgh, 1978, edited by W. Vogt and M. Mickle, Publ. Inst. Soc. Am., Pittsburgh, PA (1979).

18. F. P. Mattar, H. M. Gibbs, S. L. McCall and M. S. Feld, Phys. Rev. Lett. 46, 1123 (1981).

19. C. M. Bowden and F. P. Mattar, to be published.

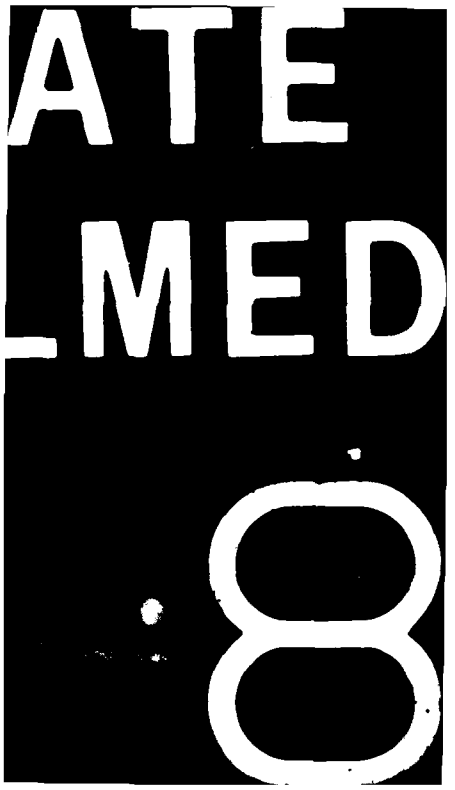
ATE
LMED
8